Proceedings of the 7th International Conference on Energy Harvesting, Storage, and Transfer (EHST'23)
Canada – June 07-09, 2023
Paper No. 127
DOI: 10.11159/ehst23.127

Natural Rayleigh Benard Convection of Bingham Fluid in Enclosure Cavity with Sinusoidal Profiles

Keddar Mohammed[1], Draoui Belkacem[1], Mebarki Brahim[1] and Medale Marc[2]
[1] Laboratory of Arid Zones Energetic - (ENERGARID), Faculty of Technology, University of Tahri Mohamed Bechar
BP 417 (08000), Bechar, Algeria
keddar.mohammed@univ-bechar.dz ; draoui.belkacem@univ-bechar.dz ;
brahim.mebarki@univ-bechar.dz
[2]Aix-Marseille University, Polytech Marseille, Energy Mechanics Dept IUSTI laboratory,
UMR 7343 CNRS-Aix-Marseille University Chateau-Gombert Technopole
5 rue Enrico Fermi 13453 MARSEILLE, Cedex 13, FRANCE
marc.medale@univ-amu.fr

Abstract **-** In this study, two-dimensional steady-state simulations of laminar natural convection of Rayleigh Benard in square enclosure were performed. The enclosure is considered to be completely filled with a yield stress fluid obeying viscoplastic model Bingham. The vertical lateral walls are thermally isolated, whereas sinusoidal temperature distributions with different amplitudes and phases are imposed over the horizontal walls. Fluid flow and heat transfer characteristics are systematically studied over a wide range of Phase deviation ϕ (0- π) and amplitude ration ε (0-1). We have fixed the Rayleigh number (Ra = 10^5), Prandtl number (Pr = 7), and finally the Bingham number (Bn = 0.5). The Navier-Stokes equations, the mass and energy conservation equations, are solved numerically using CFD software FLUENT 15. The results shows that the Nusselt number decreases with the increase of the Bingham number, and for the large values of the latter the heat transfer is done by conduction. It is also noteworthy that the increase in the phase difference and the amplitude ratio leads to the increase in the heat transfer.

Keywords**:** Natural convection, Convective flow, non-Newtonian fluid, Viscoplastic fluid, Bingham fluid, Numerical simulation, Amplitude ratio, Phase deviation

1. Introduction

The buoyancy-driven heat convection inside an enclosure has been widely investigated during the last several decades [1-2-3]. Natural convection in an enclosure may be seen in various applications such as electronic equipment cooling, building cooling and heating, solar heaters, energy drying processes etc. The classical Rayleigh–Benard convection [4] had been observed in an enclosure heated from below and cooled from above. Extensive study of the convection inside the enclosure has been reported in review articles [5–6-7-8]. One of the many studied cases is holding the horizontal walls isothermally at different temperatures while the other walls (vertical walls) are insulated to maintain the adiabatic state, for example, [9-10-11-12] investigated natural Rayleigh Benard convection of yield stress fluids. although various configurations of heated shaped objects are possible, such as cubic cavity which is totally immersed within yield stress fluid [13] sphere [14-15] and cylinder [16]. There is also one of the most classic cases which is a differentially heated cavity filled with Bingham Fluids [17-18], where the vertical walls have different temperatures while the other walls (top and bottom) are adiabatic.

The present work aims to investigate a more complicated natural Rayleigh Benard convection in an enclosure with two sinusoidal temperature profiles on the top and the bottom walls, the enclosure is considered to be completely filled with a flow stress fluid obeying the Bingham model. The results indicate that the Nusselt number decreases with the increase of the Bingham number, and for the large values of the latter the heat transfer is done by conduction, also the increase in the phase difference and the amplitude ratio leads to the increase in the heat transfer.

2. Numerical Methods

FLUENT, a commercial CFD software, provides the numerical model. Subject to the suggested boundary conditions, the conservation equations are discretized using a finite-volume technique based on the SIMPLEC algorithm. The second-

order upwind differencing method is used to discretize the equations. Finally, the convergence requirements for solving the governing equations are regarded met when the sum of the residuals is less than 10^{-5}.

2.1. Geometry and Boundary Conditions

fig 1 presents the schematic diagram of the domain which the simulations will be run. Where thermal isolation exists between the vertical lateral walls, and the horizontal walls exhibit sinusoidal temperature distributions with varying amplitudes and phases. We make certain approximations and simplifying assumptions to reduce and simplify the mathematical formulation of the model and facilitate its resolution. Two-dimensional flow is assumed to be permanent; fluid flow is assumed to be incompressible and laminar, and finally thermo-physical properties of the fluid are constant, except for apparent viscosity, which varies according to the viscoplastic model, the Boussinesq approximation.

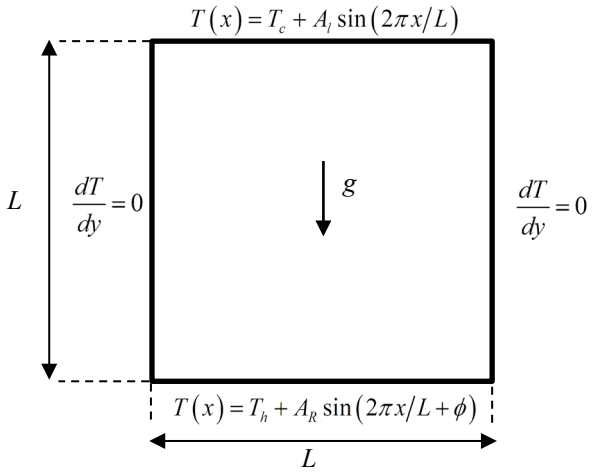

Fig. 1: Layout of the simulation domain.

2.2. Mathematical Formulation

The steady-state conservation equations for mass, momentum, and energy in incompressible fluids are as follows. Continuity equation:

$$\frac{\partial u}{\partial x} + \frac{\partial v}{\partial y} = 0 \tag{1}$$

Momentum equations:

These equations are translated according to the Navier-Stokes equations.

Following x:

$$u\frac{\partial u}{\partial x} + v\frac{\partial u}{\partial y} = -\frac{\partial p}{\partial x} + \Pr\left(2\frac{\partial^2 u}{\partial x^2} + \frac{\partial^2 u}{\partial y^2} + \frac{\partial^2 v}{\partial x \partial y}\right) + \left(2\frac{\partial \mu_a}{\partial x}\frac{\partial u}{\partial x} + \frac{\partial \mu_a}{\partial y}\frac{\partial u}{\partial y} + \frac{\partial \mu_a}{\partial y}\frac{\partial v}{\partial x}\right) \tag{2}$$

Following *y*:

$$u\frac{\partial v}{\partial x}+v\frac{\partial v}{\partial y}=-\frac{\partial p}{\partial y}+\Pr\left(2\frac{\partial^2 v}{\partial y^2}+\frac{\partial^2 v}{\partial y^2}+\frac{\partial^2 u}{\partial x\partial y}\right)$$
$$+\left(\frac{\partial \mu_a}{\partial x}\frac{\partial u}{\partial x}+2\frac{\partial \mu_a}{\partial y}\frac{\partial v}{\partial y}+\frac{\partial \mu_a}{\partial x}\frac{\partial u}{\partial y}\right)+Ra\Pr\theta \quad (3)$$

The energy equation:

$$u\frac{\partial \theta}{\partial x}+v\frac{\partial \theta}{\partial y}=\left(\frac{\partial^2 \theta}{\partial x^2}+\frac{\partial^2 \theta}{\partial y^2}\right) \quad (4)$$

These variables have been used to make the above equations dimensionless

$x=\frac{x^*}{L}$, $y=\frac{y^*}{L}$, $u=\frac{u^*L}{\alpha}$, $v=\frac{v^*L}{\alpha}$, $p=\frac{p^*L}{\rho\alpha^2}$ $\theta=\frac{T-T_C}{T_H-T_C}$

Boundary conditions are as follows:

At the top $\mathrm{u}=\mathrm{v}=0$, $\theta=\sin(2\pi \mathrm{x})$

At the bottom of the domain $\mathrm{u}=\mathrm{v}=0$, $\theta=\varepsilon\sin(2\pi \mathrm{x}+\phi)$

The vertical walls $\mathrm{u}=\mathrm{v}=0$, $\frac{\mathrm{dT}}{\mathrm{dy}}=0$

Where Ɛ = AR/ Al is the amplitude of the sinusoidal temperature which is at the bottom and at the top of the cavity, with AR being the aspect ratio and AR = H / L et Al = $T_h - T_c$

The Bingham model is governed by the following equations:

$$\begin{cases}\dot{\gamma}=0 & if \quad \tau\le\tau_0\\ \tau=\left(\mu+\frac{\tau_0}{\dot{\gamma}}\right)\dot{\gamma} & if \quad \tau>\tau_0\end{cases} \quad (5)$$

Dimensionless Rayleigh number:

$$Ra=\frac{\rho^2 Cp\, g\beta\Delta T\, L^3}{\mu\lambda}=Gr\Pr \quad (6)$$

Dimensionless Grashoff number:

$$Gr=\frac{\rho^2 g\beta\Delta T\, L^3}{\mu^2} \quad (7)$$

Dimensionless Prandtl number:

$$\Pr=\frac{\mu Cp}{\lambda} \quad (8)$$

Dimensionless Bingham number:

$$Bn=\frac{\tau_0}{\mu}\sqrt{\frac{L}{g\beta\Delta T\, L}} \quad (9)$$

2.3 Validation

To validate our results, we compared them with those of the literature, namely the work of references [8] and [17]. A good argument has been noted between our numerical results and those of the articles [8] and [17].

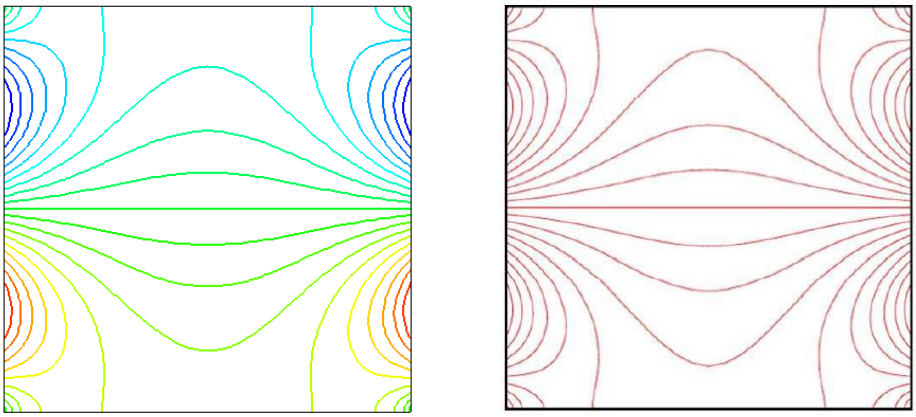

Fig 2: Comparison of numerical result obtained (left) with [8] (right) of the Effect of Rayleigh number on the isotherms at Ra = 10^3, Bn = 0, Pr = 0.7, ϕ = 0 and ε = 1.

Table 1: Nusselt validation [17]

	Bn = 1	Bn = 3	Bn = 6	Bn = 9	Bn = 18	Bn = 27
Ra = 10^5						
Huilgol [17]	3.303	3.263	3.083	2.898	2.402	2.143
Present work	3.305	3.265	3.083	2.900	2.403	2.140

3 Results and Discussion

3.1 Effect of Phase Deviation

Fig 3 shows the variations of streamlines and isotherms with a phase difference ranging from 0 to π. The streamlines are in the shape of one cell at ϕ = 0, but the shape of this cell changes and deforms at ϕ =π/4. At ϕ =π /2, we see the appearance of a tiny cell on the bottom of the right side, the shape of the streamlines has changed from one cell to two with differing forms. The size of the bottom corner cell grows in proportion to the phase difference. When ϕ =π, the flow structure in the enclosing halves is two almost similar cells. The isotherms along the top wall are largely conserved over the phase deviation variation cycle, whereas the isotherm distributions along the bottom wall change.

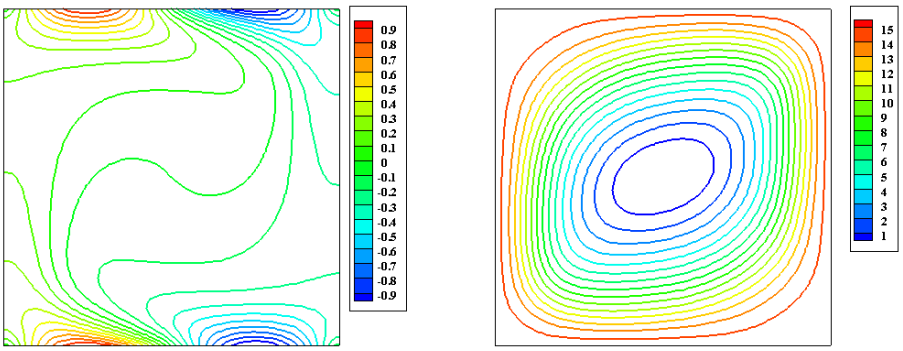

$\phi = 0$

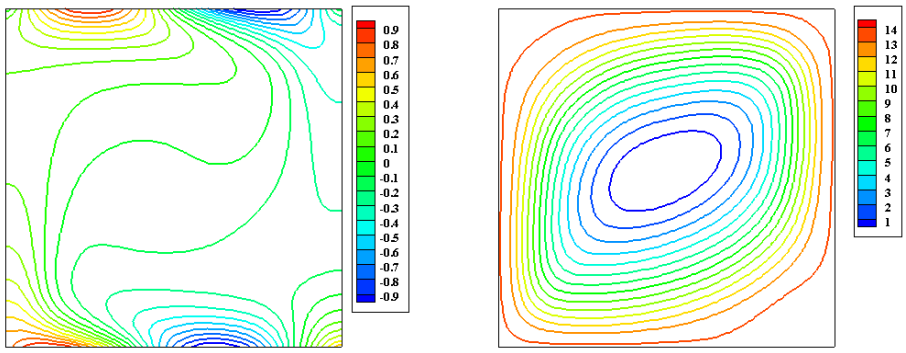

$\phi = \pi/4$

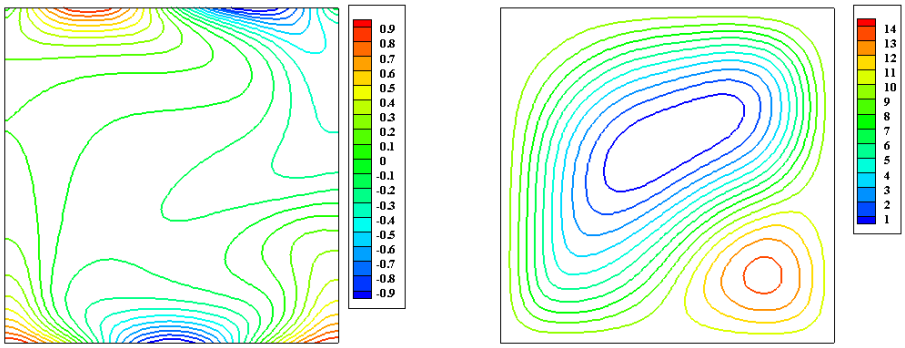

$\phi = \pi/2$

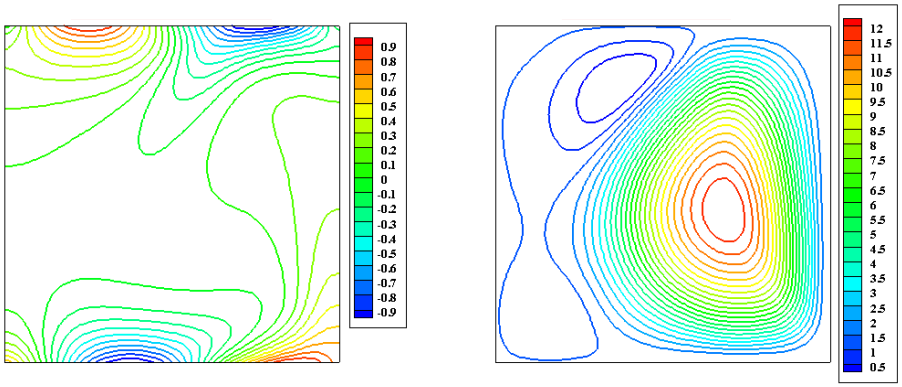

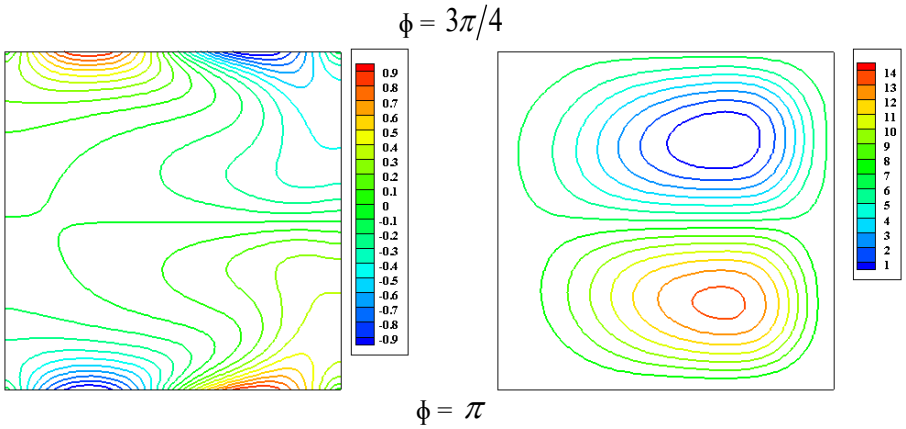

Fig 3: Contours of isotherms of Bingham's three-dimensional fluid model for Ra = 10^5; Bn = 0.5 ; Pr = 7; Ɛ = 1.

3.2. Effect of Amplitude

Fig 4 illustrates the changes of the streamlines and isotherms in terms of the amplitude ratio. The streamlines are in the shape of a single cell, but its shape changes and deforms as the amplitude ratio increases. At Ɛ = 0, we noticed that heat transfer occurs only the top wall and not the bottom, as Ɛ increases more and more isotherms appear along the bottom wall and thus heat transfer across the bottom wall increases. Finally, we can say that the increase of Ɛ improves the heat transfer.

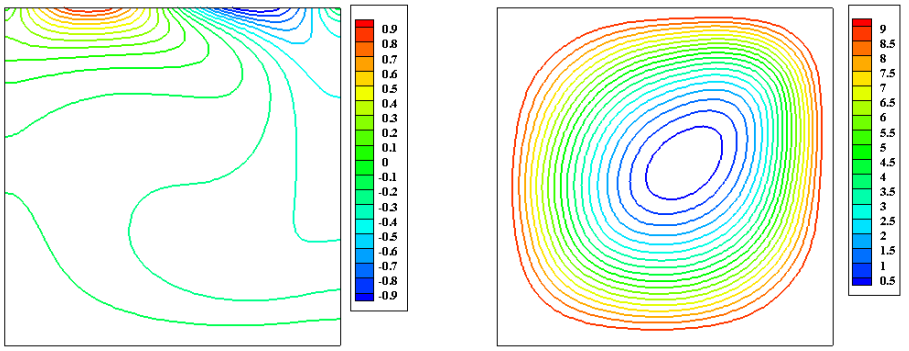

(a) Ɛ = 0

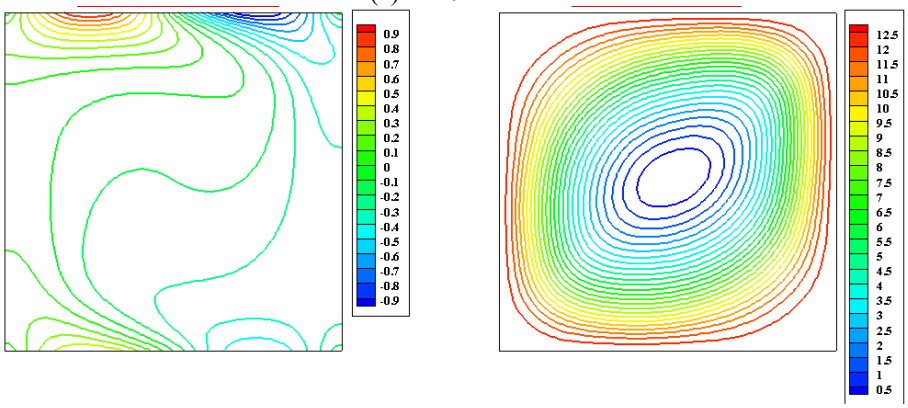

(b) Ɛ = 0,5

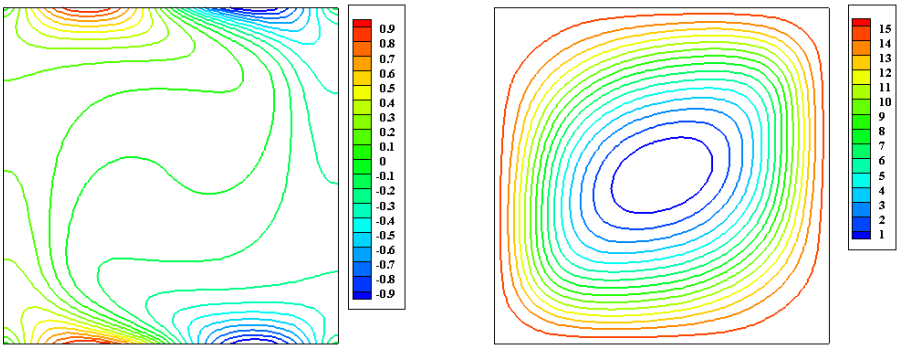

(c) Ɛ = 1

Fig 4 : Contours of isotherms (left) and streamlines (right) of the Bingham fluid for Ra = 10^5 ; Bn = 0,5 ; Pr = 7 ; ϕ = 0

3.3 Heat Transfer Quantification

The variation of Nusselt number is shown in figs 5 and 6. The results reveal that the Nusselt number drops as the Bingham number increases, and that for large values of the latter, heat transmission occurs by conduction. It is also worth noting that increasing the phase difference and amplitude ratio increases heat transmission.

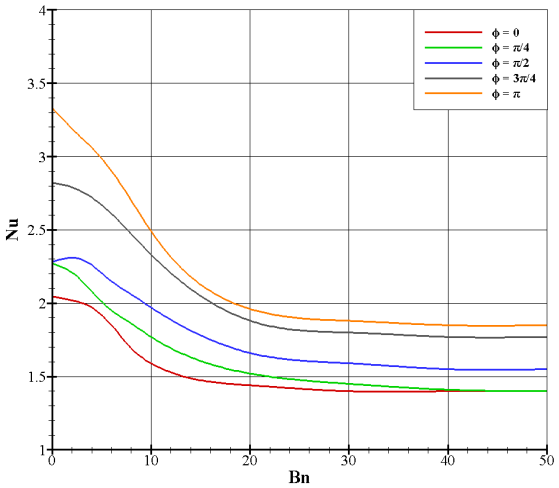

Fig 5: Effect of the phase deviation (ϕ) on the average Nusselt for Ra = 10^5, Pr = 0.1 and Ɛ = 1.

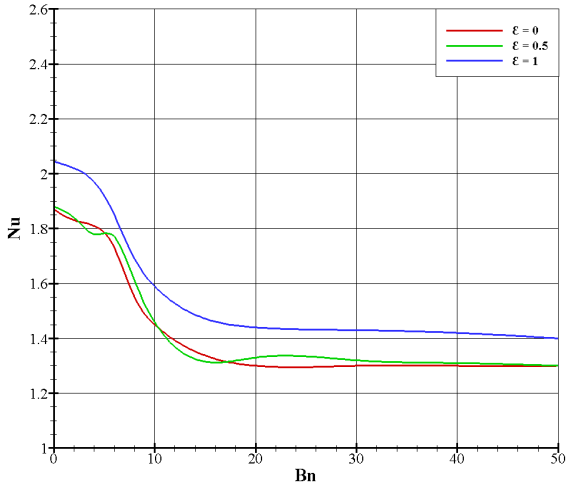

Fig 6: Effect of the amplitude ratio (Ɛ) on the average Nusselt for Ra = 10^5, Pr = 0.1 and $\phi = 0$.

4 Conclusion

This work concerns a numerical study of the two-dimensional natural Rayleigh Benard convection of a non-Newtonian viscoplastic fluid. The viscoplastic behaviour is described by the Bingham model. The two-dimensional convective flow considered is confined in a cavity, where vertical walls are thermally insulated and the horizontal walls have two sinusoidal temperatures. The Navier-Stokes equations, the mass and energy conservation equations, are solved numerically using an industrial numerical simulation code CFD: FLUENT.

- The Nusselt number decreases with the increase of the Bingham number, and for the large values of the latter the heat transfer is done by conduction.
- The increase in the phase difference leads to the increase in the heat transfer, with regard to the influence of the phase deviation on the Nusselt. It is observed that from the values, the heat transfer rate is improved for $\phi = \pi$.
- Heat transfer increases as the amplitude ratio increases. The heat transfer rate for $\varepsilon = 1$ is higher than in the other cases.

5 References

[1] Sadeghi, M. S., Tayebi, T., Dogonchi, A. S., Nayak, M. K., & Waqas, M. (2020). Analysis of thermal behavior of magnetic buoyancy-driven flow in ferrofluid–filled wavy enclosure furnished with two circular cylinders. *International Communications in Heat and Mass Transfer*, *xxxx*, 104951.

[2] Memon, A., Mishra, G., & Gupta, A. K. (2020). Buoyancy-driven melting and heat transfer around a horizontal cylinder in square enclosure filled with phase change material. *Applied Thermal Engineering*, *181*(May), 115990.

[3] Yang, C., Gao, T., Li, A., & Gao, X. (2021). Buoyancy-driven ventilation of an enclosure containing a convective area heat source. *International Journal of Thermal Sciences*, *159*(November 2019), 106551.

[4] A. Bejan. Convective Heat Transfer, Wiley New York, 1984,

[5] G. de Vahl Davis, Natural convection of air in a square cavity: a bench mark numerical solution, Int. J. Numer. Methods Fluids 3 (1983) 249–264.

[6] A.F. Emery, J.W. Lee, The effects of property variations on natural convection in a square cavity, J. Heat Transfer 121 (1999) 57–62.

[7] O. Aydın, A. Unal, T. Ayhan, Natural convection in rectangular enclosures heated from one side and cooled from above, Int. J. Heat Mass Transfer 42 (1999) 2345–2355.

[8] Deng H.Q., Chang. J.J. (2008). Natural convection in a rectangular enclosure with sinusoidal temperature distributions on both side walls, *Numerical Heat Transfer, Part A*, Vol. 54, pp. 507-524.

[9] Turan, O., Yigit, S., & Chakraborty, N. (2017). Critical condition for Rayleigh-Bénard convection of Bingham fluids in rectangular enclosures. *International Communications in Heat* and mass transfer, 86(june), 117–125.
[10] Aghighi, M. S., Ammar, A., Metivier, C., & Gharagozlu, M. (2018). Rayleigh-Bénard convection of Casson fluids. *International Journal of Thermal Sciences*, *127*(February 2017), 79–90.
[11] Yigit, S., Chen, S., Quinn, P., & Chakraborty, N. (2016). Numerical investigation of laminar Rayleigh-Bénard convection of Bingham fluids in square cross-sectioned cylindrical enclosures. International journal of thermal sciences, 110, 356–368.
[12] Sun, M. H., Wang, G. B., & Zhang, X. R. (2019). Rayleigh-Bénard convection of non-Newtonian nanofluids considering Brownian motion and thermophoresis. *International Journal of thermal sciences*,*139*(February),312–325.
[13] Yigit, S., Hasslberger, J., Chakraborty, N., & Klein, M. (2020). Effects of Rayleigh-Bénard convection on spectra of viscoplastic fluids. *International Journal of Heat and Mass Transfer*, *147*, 118947.
[14] Guiquan Wang, Luca Santelli, Roberto Verzicco, Detlef Lohse and Richard J.A.M. StevensOff-centre gravity induces large-scale flow patterns in spherical Rayleigh–Bénard convection, Journal of Fluid Mechanics, Volume 942, 10 July 2022, A21
[15] Yanagisawa, T., & Yamagishi, Y. (2005). Rayleigh-Benard convection in spherical shell with infinite Prandtl number at high Rayleigh number. *J. Earth Simulator*, *4*(December), 11-17.
[16] Sadeghi, M. S., Tayebi, T., Dogonchi, A. S., Nayak, M. K., & Waqas, M. (2020). Analysis of thermal behavior of magnetic buoyancy-driven flow in ferrofluid–filled wavy enclosure furnished with two circular cylinders. *International Communications in Heat and Mass Transfer*, *xxxx*, 104951.
[17] Huilgol, R. R., & Kefayati, G. H. R. (2015). Natural convection problem in a Bingham fluid using the operator splitting method. *Journal of Non-Newtonian Fluid Mechanics*, *220*, 22–32.
[18] Turan, O., Chakraborty, N., & Poole, R. J. (2010). Laminar natural convection of Bingham fluids in a square enclosure with differentially heated side walls. *Journal of Non-Newtonian Fluid Mechanics*, *165*(15–16), 901–913.